Int. J. Electrochem. Sci., 15 **(2020)** 6991 – 7000, doi: 10.20964/2020.07.84

International Journal of
ELECTROCHEMICAL
SCIENCE
www.electrochemsci.org

Effects of Polyoxyethylene Ether Addition on the Nucleation and Microtopography of Zinc Electrodeposited in a Neutral Electrolyte

Duoqiang Zhao[*], *Yafei Jie, Yongming Chen, Chaobo Tang, Jing He and Shenghai Yang*

School of Metallurgy and Environment, Central South University, National Engineering Laboratory for High Efficiency Recovery of Refractory Nonferrous Metals, Changsha 410083, China
[*]E-mail: zhdq11261987@163.com

Received: 11 March 2020 / *Accepted:* 8 May 2020 / *Published:* 10 June 2020

This work investigated the mechanism underlying the effect of polyoxyethylene ether (PEO-1100) on Zn nucleation and growth in a neutral solution (5 M NH_4Cl). The mechanism underlying the modification of the Zn morphology in a Zn^{2+}-NH_4^+-Cl^- solution by PEO-1100 was studied through cathodic polarization, cyclic voltammetry, chronoamperometry, X-ray diffraction (XRD), metallographic examination, and scanning electron microscopy (SEM). A dendrite-free Zn film was obtained at a current density of 40 mA cm^{-2}. The internal microstructure of Zn in the presence and absence of PEO-1100 was observed through metallographic examination and SEM. XRD revealed that the Zn crystal growth exhibited a preferential orientation in the presence of PEO-1100. The reduction kinetics of zinc were inhibited by the addition of PEO-1100. The effects of PEO-1100 on Zn nucleation and the overpotential of Zn deposition were observed.

Keywords: Zinc electrodeposition, Neutral electrolyte, Dendritic growth, Internal microtopography

1. INTRODUCTION

In metallurgical industries, cathodic zinc (Zn) is mainly electrotwinned in a sulfuric acid system [1]. Metallic Zn is a promising anode material for secondary rechargeable batteries, given its high energy density, good reversibility, and economic feasibility [2]. Zn dendrite growth is harmful to batteries and metallurgical and electroplating processes. A smooth sediment layer is expected to be obtained [3-5]. Dendrites can easily cause short circuits in batteries and metallurgical processes, reduce corrosion resistance and wear resistance during electroplating, and affect the appearance of the final electroplating product. Organic additives are used to inhibit the growth of dendritic crystals in traditional acidic and alkaline systems [6,7]. The addition of organic compounds can reduce the grain size of dendritic crystals [8]. Glue, gelatin, ammonium base salts, and polyethylene glycol are commonly used as additives in Zn

electrochemical research [9-12].

Organic additives can change the growth orientation and nucleation mechanism of crystals [13]. Nucleation and crystal growth play decisive roles in microstructural development during electrodeposition. If nucleation and crystal growth are ordered, the growth of dendrites will be inhibited, the numbers of pores inside the sedimentary layer will drastically decrease, and the density of the sedimentary layer will increase.

The addition of organic additives can change the internal microscopic morphology of Zn deposits. The internal microscopic morphology of Zn deposits has a considerable effect on the formation of dendrites and the density of the sedimentary layer [14]. XRD has been used to detect the growth orientation of Zn and calculate the Zn grain size [15]. The internal structure of the Zn deposit layer has rarely been directly observed. Only the microstructure of the front side of the sediment layer, not the internal microstructure of the side of the sediment layer, has been observed through scanning electron microscopy (SEM) [16]. The arrangement of Zn crystal grains and the location of pores can be directly inferred from the internal microstructure of the sediment layer.

Numerous studies on the electrochemical behavior of Zn under acidic and basic conditions have been conducted. Nevertheless, the effect of polyoxyethylene ether (PEO-1100, whose main functional groups are -C-O-C- and -O-H and molecular weight is 1100) on the electrochemical behavior of Zn deposition in a neutral system has not been reported. The internal microstructure of Zn deposits has also been rarely visualized. In this work, the effect of PEO-1100 on the electrochemical behavior of Zn under neutral conditions was studied, and the internal structure of the Zn deposit was characterized.

The following research was conducted to explore the effect of organic additives on the electrochemical behavior and microstructure of the Zn sedimentary layer in a neutral system.

2. EXPERIMENTAL

Electrolyte solutions were prepared by the reaction of ZnO (10 g L^{-1} Zn^{2+}), $ZnCl_2$ (15 g L^{-1} Zn^{2+}), and NH_4Cl (267.45 g L^{-}) in water (analytical grade, Shanghai Chemistry Reagent Company, China). Cathodic polarization and cyclic voltammetry were performed at 45 °C with a scan rate of 1 mV s^{-1}. Chronoamperometry was performed at 45 °C. The samples used for XRD, the metallographic examination, and SEM testing were prepared at 45 °C and a current density of 40 mA cm^{-2} and with an animal glue concentration of 0.2 g L^{-1}. PEO-1100 and the electrolyte were mixed well prior to the initiation of the electrochemical experiment. The electrochemical setup was a conventional three-electrode cell. A glassy carbon plate (chronoamperometry) or Zn plate (cathodic polarization and cyclic voltammetry) with a surface area of 0.225 cm^2 was used as the working electrode. A Pt plate with a surface area of 1.0 cm^2 was used as the counter electrode, and a saturated calomel electrode was used as the reference electrode. The working electrode was enclosed in epoxy resin, polished to a mirror finish with 3 mm abrasive paper, and then washed with acetone and alcohol. The electrochemical experiments were controlled by using a Galvanostat CHI660C system (CH Instrument, China) linked to a computer.

The XRD results were obtained for the Zn films with a RIGAKU-TTRIII (Japan) D/max2550 diffractometer with a slit width of 0.25° using Cu Kα radiation (40 kV, 200 mA, $\lambda = 0.154$ nm), and data

were collected over the 2θ range of 10° to 80°. SEM was performed using a TESCAN MIRA3 instrument (Czech Republic). The front and side of the Zn deposits must be ground to a mirror finish and then etched with dilute HCl prior to SEM observation.

3. RESULTS AND DISCUSSION

The cathodic polarization curves obtained in the presence or absence of PEO-1100 are shown in Fig. 1. Zn deposition is characterized by a slight increase in current. The rapid increase in current when the potential is negatively shifted to a certain value corresponds to the reduction of Zn ions. The onset potential in the presence of PEO-1100 is drastically lower than that in the absence of PEO-1100. This result indicates that PEO-1100 can enhance cathodic polarization and inhibit Zn electrodeposition.
The Tafel equation is as follows:

$$\eta = a + b \lg j \quad (1)$$

$$a = -\frac{2.303RT}{\alpha nF} \lg j_0 \quad (2)$$

$$b = \frac{2.303RT}{\alpha nF} \quad (3)$$

where j_0 is the exchange current density, η is the overpotential, α is the transfer coefficient, T is the temperature, R is a constant 8.315, and nF is the molar charge of zinc.

The effects of the PEO-1100 concentration on the kinetic parameters calculated from Fig. 1 are given in Table 1. The equilibrium potential (E_e), transfer coefficient (α) and exchange current density (j_0) decrease as the concentration of the additive increases. The reduction kinetics of zinc are inhibited due to the addition of PEO-1100. These changes likely stemmed from the occupation of H_2O molecules by PEO-1100 on the zinc electrode surface [17].

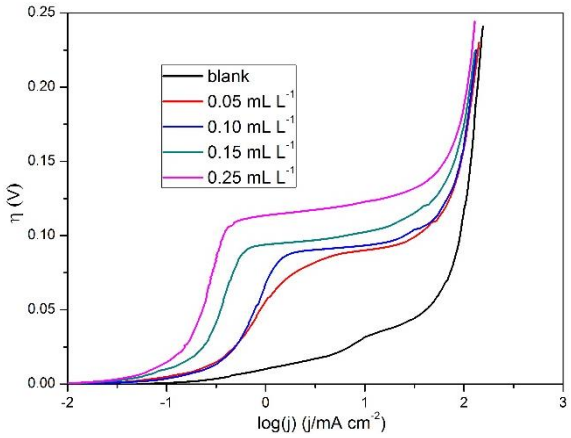

Figure 1. Cathodic polarization plots obtained in the presence of various PEO-1100 concentrations

Table 1. Kinetic parameters

PEO concentration /(mL L^{-})	Equilibrium potential E_e/(V)	Tafel slope b	Transfer coefficient $\alpha \cdot 10^{-3}$	Exchange current density, $j_0 \cdot 10^{-3}$/(mA cm^{-2})
0	-1.108	0.028	1.111	0.573
0.05	-1.119	0.089	0.353	0.527
0.1	-1.124	0.148	0.213	0.513
0.15	-1.127	0.188	0.168	0.492
0.25	-1.128	0.247	0.127	0.490

The similar shapes of the cyclic voltammetry curves (Fig. 2) obtained in the presence or absence of PEO-1100 indicate that the basic process of the electrochemical reaction has not been changed by the addition of PEO-1100. The peak current decreases drastically with the addition of PEO-1100. The decrease in the peak current becomes increasingly pronounced as the concentration of PEO-1100 is increased. The corrosion current shows a similar trend. The adsorption of PEO-1100 on the electrode surface blocks Zn deposition and corrosion.

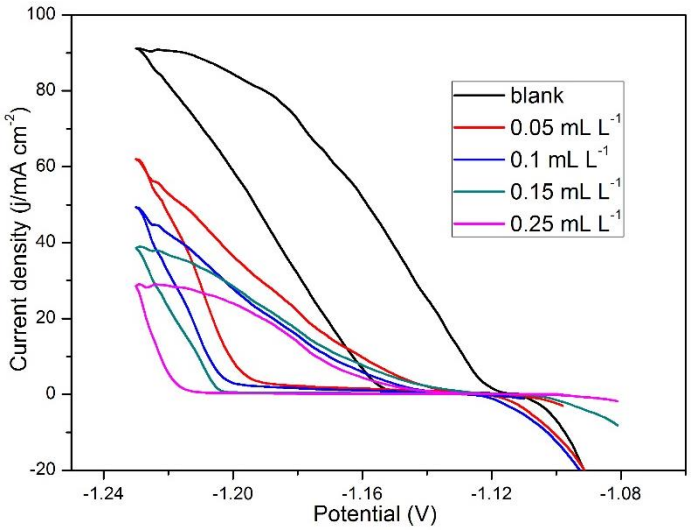

Figure 2. Cyclic voltammetry plot obtained in the presence of various PEO-1100 concentrations

Chronoamperograms (Fig. $3a_1$ and a_2) are used to study the nucleation and growth mechanism that occur in the initial Zn deposition process. The charging of the electric double layer is represented by an instantaneous increase to a specific value and subsequent reduction to 0 mA [18]. Current peak generation is attributed to the formation of many crystal nuclei. The current decreases to a stable value after peaking. This behavior indicates that nucleation and grain growth have reached equilibrium.

The nucleation mechanism involved in the electrodeposition of a metal onto a foreign substrate is classified as either instantaneous or progressive, and the growth mechanism is termed as three-

dimensional (3D) island growth. In instantaneous nucleation, all points that can be nucleated are activated instantaneously, and nucleation occurs rapidly. In progressive nucleation, the points are activated gradually, and nucleation occurs while other clusters are growing [19,20]. The Scharifer-Hills model is the most used model. The Scharifer-Hills model provides a simple approach for distinguishing instantaneous nucleus growth and progress. The theoretical transients of instantaneous and progressive nucleation achieved with 3D growth under diffusion control are given by equations 4 and 8 [21,22]:

Instantaneous nucleation:

$$(\frac{j}{j_m})^2 = 1.9542(\frac{t}{t_m})^{-1}\{1-\exp[-1.2564(\frac{t}{t_m})]\}^2 \quad (4)$$

$$t_m = \frac{1.2564}{N\pi kD} \quad (5)$$

$$j_m^2 t_m = 0.1629(nFC)^2 D \quad (6)$$

$$k = \sqrt{8\pi CM/\rho} \quad (7)$$

Progressive nucleation:

$$(\frac{j}{j_m})^2 = 1.2254(\frac{t}{t_m})^{-1}\{1-\exp[-2.3367(\frac{t}{t_m})^2]\}^2 \quad (8)$$

$$t_m = \sqrt{\frac{4.6733}{AN_\infty \pi k` D}} \quad (9)$$

$$j_m^2 t_m = 0.2598(nFC)^2 D \quad (10)$$

$$k` = \frac{4}{3}\sqrt{8\pi CM/\rho} \quad (11)$$

where j and t are the current density and time, respectively, j_m is the maximum value of the current density, and t_m is the time when the current reaches its maximum value. nF is the molar charge of the depositing species, D is its diffusion coefficient, C its concentration in mol cm^{-3}, M its molecular weight and ρ its density, N is the number of nuclei, and A is the steady state nucleation rate constant per site.

The curves corresponding to the instantaneous nucleation and progressive nucleation models are shown in Fig. $3b_1$ and Fig. $3b_2$, respectively. The nucleation mechanism changes from instantaneous nucleation to progressive nucleation in the presence of PEO-1100. In an acid system, cetyltrimethylammonium bromide also can change the nucleation mechanism from instantaneous nucleation to progressive nucleation [23]. The electrochemical properties of the electrode change upon the addition of PEO-1100. The effects of the PEO-1100 concentration on the diffusion coefficient (D) and number of nuclei (N) calculated from Fig. 3 are given in Table 2. The quantity poles of the diffusion coefficient (D) and nuclei (N) are 10^{-5} and 10^5, respectively. The increase in the D and N values with the negative shift in the electric potential indicates that the overpotential has a great effect on the nucleation mechanism [24]. The diffusion coefficient and number of nuclei are decreased by the addition of PEO-1100.

Table 2. Diffusion coefficient (D) and number of nuclei (N)

PEO-1100 0.1 mL L^{-1}			Absence of PEO-1100		
Potential V	D/(×$10^{-5}$$cm^2$·$s^-$)	N/(×$10^5$$cm^{-2}$)	Potential V	D/(×$10^{-5}$$cm^2$·$s^-$)	N/(×$10^5$$cm^{-2}$)
-1.27	1.72	0.61	-1.22	1.48	0.81
-1.28	1.98	0.71	-1.23	1.55	1.09
-1.29	2.22	0.72	-1.24	1.65	1.71

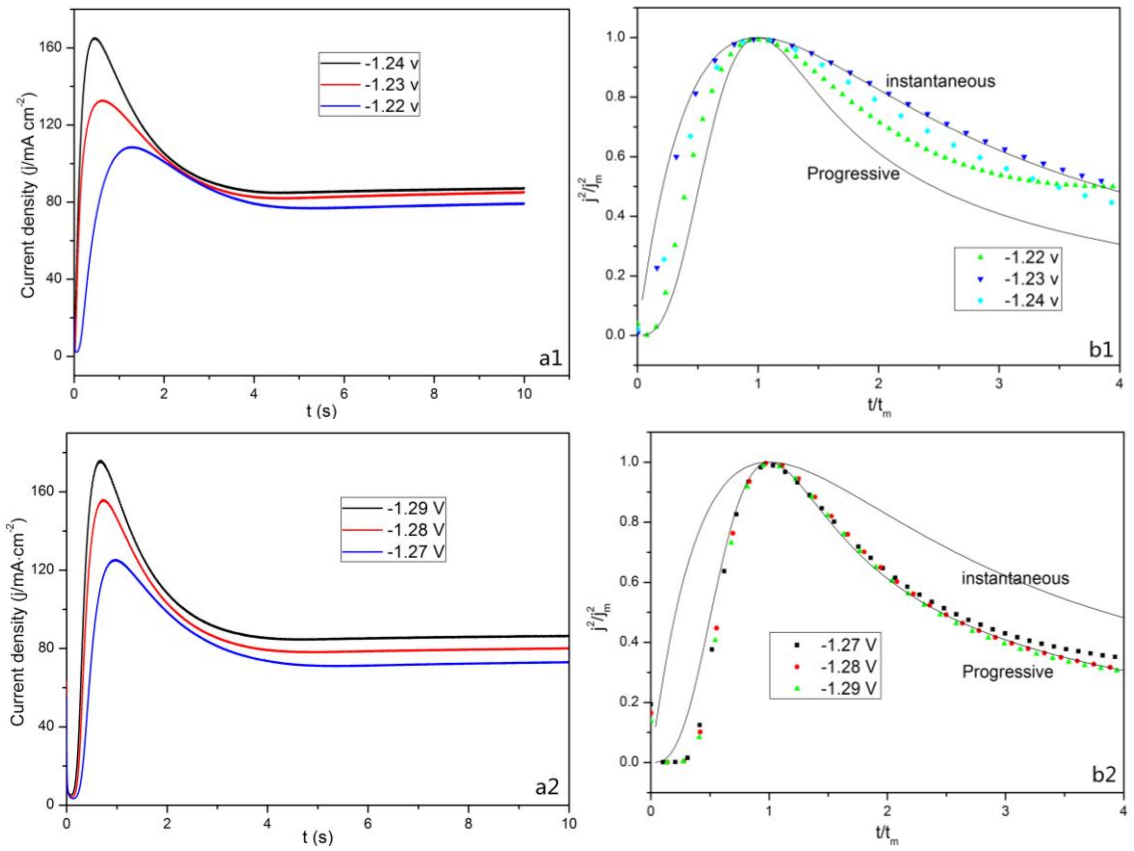

Figure 3. Chronoamperograms obtained for Zn deposition at different potentials (a1, a2) and a comparison of the dimensionless experimental model with the dimensionless theoretical models for 3D nucleation (b1, b2) (a1, b1 in the absence of PEO-1100, a2, b2 0.1 mL L^{-1} PEO-1100)

Cross-sectional SEM images obtained in the presence of 2.5 mL L^{-1} PEO-1100 are shown in Fig. 4(a). A visible grain interface and grains with uniform sizes are clearly shown. The original grains grow in one direction to sizes of approximately 800 nm × 200 nm. New grains form along the edges of the original grains. Zn is easily reduced and deposited at the grain edges because of the high activity and low steric hindrance at the grain edges. A dense Zn deposit is formed through reciprocal growth. Crystal growth mainly occurs along two directions. The angle between these two directions is approximately 115°, as obtained by direct measurement. The orderly growth pattern exhibited by the Zn grains indicates that the activities of certain crystal faces are inhibited by the addition of PEO-1100. The mechanism is similar to the highly oriented pyrolytic graphite surface partially covered by a gelatine film which blocks

the steps edges and surface defects [13].

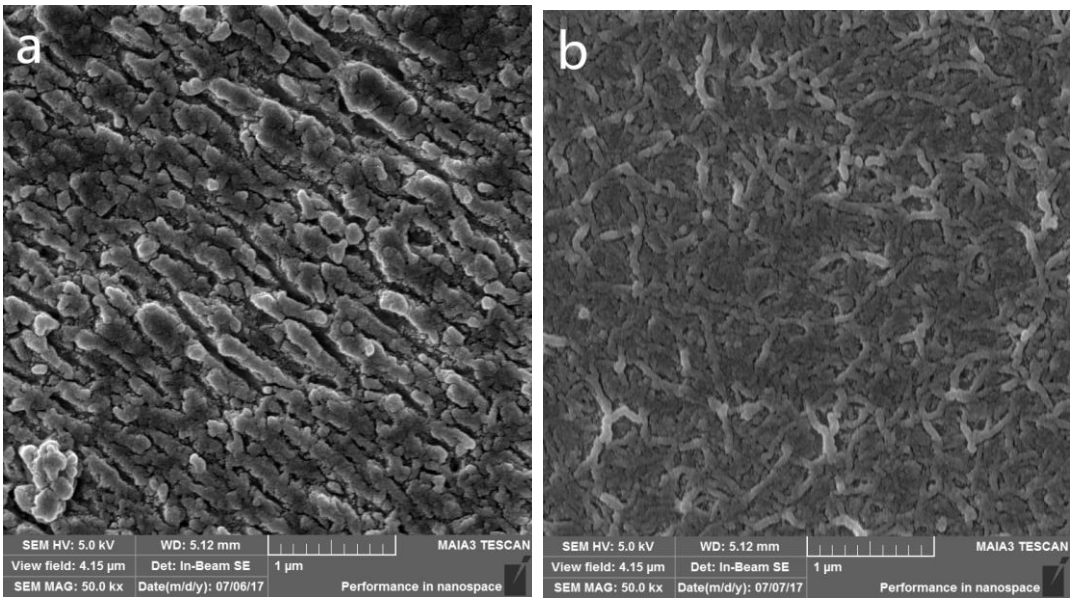

Figure 4 Cross-sectional SEM images (polished and etched) obtained in the presence of 2.5 mL L^{-1} PEO-1100 (a) and in the absence of PEO-1100 (b)

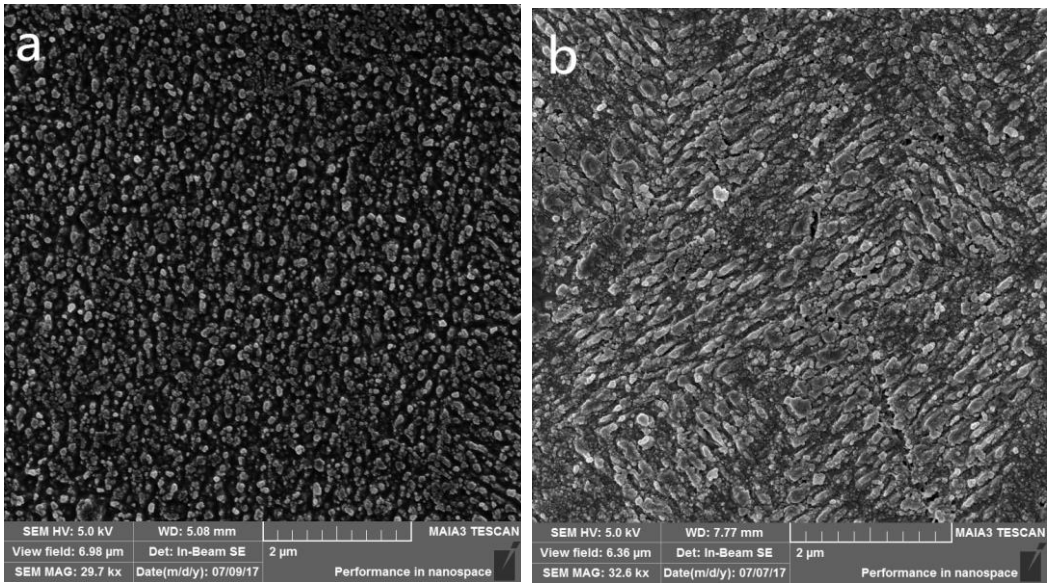

Figure 5. Front SEM images (polished and etched) obtained in the presence of 2.5 mL L^{-1} PEO-1100 (a) and in the absence of PEO-1100 (b)

Cross-sectional SEM images obtained in the absence of PEO-1100 are shown in Fig. 4(b). The crystals present disorderly growth. Nonuniform and irregularly shaped grains are produced. A Zn deposit with dense and ordered internal structures is hard to obtain. The negligible variation in the activity of

each crystal plane induces Zn grain growth along a random direction. This disordered growth becomes increasingly severe during growth and eventually results in the production of Zn particles with a loose structure. Large quantities of dendrites are also generated as disorder intensifies during growth. A similar phenomenon was found during zinc deposition on iron substrates from alkaline zincate solutions [25].

The front SEM image acquired in the presence of 2.5 mL L^{-1} PEO-1100 is shown in Fig. 5(a). As shown in Fig. 4(a), Zn is present in the form of columnar crystals (with dimensions of approximately 100 nm × 200 nm × 800 nm). Addition of PEG gives rise to Cu deposit that is changed to a columnar growth [26]. The grain boundaries (Fig. 5(a)) are clear, and the grain surface follows a certain orientation [27]. The front SEM image acquired in the absence of PEO-1100 is shown in Fig. 5(b). The front sides of the grains are highly irregular, and numerous corroded components are present between the crystal grains. It is shown that large gaps exist between the crystal grains. Several holes exist between the grains, and even cracks are present in some places. The numbers of holes and cracks increase as the duration of electrodeposition is prolonged. The formed Zn deposit is loose and cannot be plated.

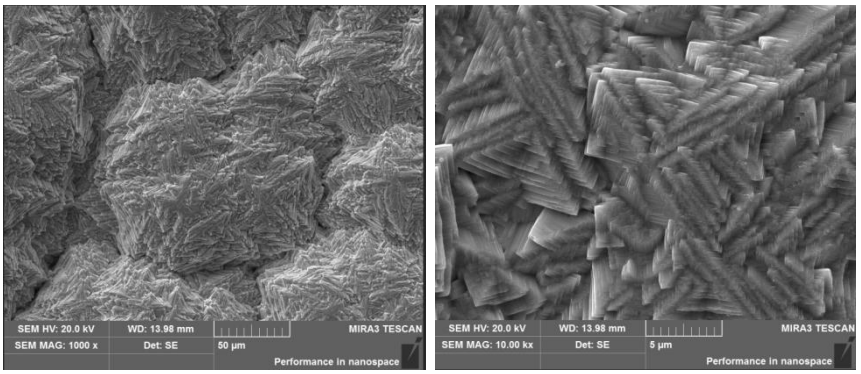

Figure 6. Front SEM images (unpolished and unetched) acquired in the presence of 2.5 mL L^{-1} PEO-1100

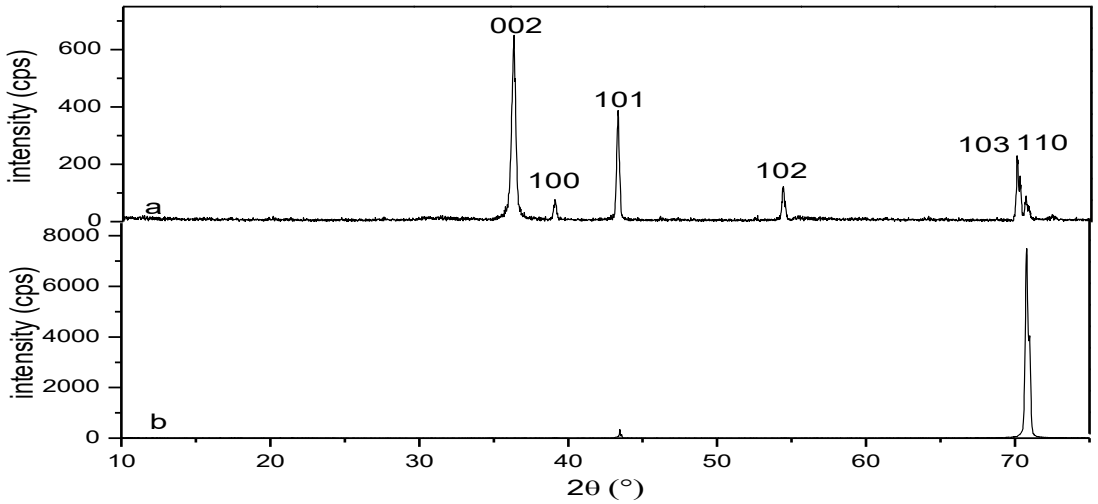

Figure 7. XRD images acquired in the absence of 2.5 mL L^{-1} PEO-1100 (a) and the presence of PEO-1100 (b)

As shown in Fig. 6, Zn is stacked in layers in the form of columnar crystals. This finding is

consistent with that shown in Fig. 5. The grains grow into columnar crystals that demonstrate a linear and regular arrangement. Almost no irregular holes are found between the columnar grains. The grain boundaries are highly pronounced at the grain boundaries in both directions. This situation will become obvious over time, and a clear transition zone is observed in the SEM images. The nucleation number, position and mechanism achieved with and without PEO-1100 are different because the additive changes the property of the active sites. In the sunken region, the activity is weakened, and the transfer speed of the material slows down [28]. This phenomenon will become increasingly obvious during the process of grain growth. The macroscopic appearance reveals a high-low intermediate macroscopic shape on the surface of the zinc plate [29,30].

As shown in Fig. 7, the growth of Zn on the 110 lattice plane intensifies with the addition of PEO-1100 [31]. This result is consistent with that shown in Fig. 5. The grains exhibit a disordered arrangement because the direction of grain growth is random in the absence of PEO-1100. The grains are pressed against one another, and many caves are formed during the growth of the grains in the absence of PEO-1100. The columnar crystals that are curved and earthworm-like gradually form, and the grain boundaries are unclear (Fig. 4b). Many caves are formed between the grains. The trend of random growth will become increasingly obvious over time. The resulting products are loose granular dendrites [32].

4. CONCLUSIONS

This work investigated the mechanism underlying the effect of PEO-1100 on Zn nucleation and growth in a neutral solution. Dendrite-free Zn was successfully electrodeposited in the presence of PEO-1100 in a neutral solution. The adsorption of PEO-1100 on the surface of the electrode modified nucleation and grain growth. The addition of PEO-1100 can enhance cathodic polarization and hinder Zn electrodeposition but did not change the basic processes of the electrochemical reaction. The reduction kinetics were inhibited because the exchange current density and coefficient decreased due to the additive. The nucleation mechanism changed from instantaneous to progressive with the addition of PEO-1100. The cross-sectional and front SEM images show that Zn is present in the form of columnar crystals (with dimensions of approximately 100 nm × 200 nm × 800 nm). The grain size is uniform, and Zn crystals grow along two directions [lattice planes 110 and 101].

ACKNOWLEDGEMENTS
This work was supported financially by the National Natural Science Foundation of China (Grant No. 51704107).

References

1. P. Guillaume, N. Leclerc, C. Boulanger, J.M. Lecuire, F. Lapicque, *J. Appl. Electrochem*., 37 (2007) 1237
2. C. Yang, Z.J. Zhang, Z.L. Tian, Y.Q. Lai, K. Zhang, J. Li, *Electrochim. Acta*, 258 (2017) 284

3. M. Xu, D.G. Ivey, W. Qu, Z. Xie, *J. Power Sources*, 274 (2015) 1249
4. Z.M. Xia, S.H. Yang, M.T. Tang, *RSC Adv*., 5 (2015) 2663
5. V. Caldeira, R. Rouget, F. Fourgeot, J. Thiel, F. Lasoste, L. Dubau, M. Chatenet, *J. Power Sources*, 350 (2017) 109
6. O. Aaboubi, J. Douglade, X. Abenaqui, R. Boumedmed, J. VonHoff, *Electrochim. Acta*, 56 (2011) 7885
7. J.L. Ortiz-Aparicio, Y. Meas, G. Trejo, R. Ortega, T.W. Chapman, E. Chainet, *J. Appl. Electrochem.*, 43 (2013) 289
8. J.C. Hsieh, C.C. Hu, T.C. Lee, *Surf. Coat. Tech*., 203 (2009) 3111
9. D.J. Mackinnon, R.M. Morrison, J.E. Mouland, P.E. Warren, *J. Appl. Electrochem*., 20 (1990) 728
10. B.C. Tripathy, S.C. Das, P. Singh, G.T. Hefter, *J. Appl. Electrochem*., 29 (1999) 1229
11. J.C. Ballesteros, P. Diaz-ArÍsta, Y. meas, R.Ortega, G.Trejo, *Electrochim. Acta*, 52 (2007) 3686
12. N. sorour, W. Zhang, E. Ghali, G. Houlachi, *Hydrometallurgy*, 171 (2017) 320
13. A.E. Alvarez, D.R. Salinas, *J. Electroanal. Chem*., 566 (2004) 393
14. K. Raeissi, A. Saatchi, M.A. Golozar, *J. Appl. Electrochem*., 33 (2003) 635
15. Y.L. Zhu, Y. kozuma, Y. katayama, T. Miura, *Electrochim. Acta*, 54 (2009) 7502
16. S. Ibrahim, A. bakkar, E. Ahmed, A. Selim, *Electrochim. Acta*, 191 (2016) 724
17. A. R. El-sayed, H.S. Mohran, H.M.A. *El-lateef, Corros. Sci*., 52 (2010) 1976
18. M.H. Hölzle, U. Retter, D.M. kolb, *J. Electroanal. Chem*., 371 (1994) 101
19. A. Sahari, A. Azizi, N. Fenineche, G. Schmerber, A. Dinia, *Surf. Rev. Let.*, 12 (2005) 391
20. G. Oskam, J.G. Long, A. Natarajan P.C. Searson, *J. Phys. D Appl. Phys.*, 31 (1998) 1927
21. B. Scharifker, G. Hills, *Electrochim. Acta*, 28 (1983) 879
22. B.R. Scharifker, J. Mostany, *J. Electroanal. Chem*., 177 (1984) 13
23. K.O. Nayana, T.V. Venkatesha, *J. Electroanal. Chem.*, 663 (2011) 98
24. G. Gunawardena, G. Hills, I. Montenegro, B. Scharifker, J. Electroanal. Chem. interfacial electrochem., 138 (1982) 255
25. L. Yuan, Z.Y. Ding, S.J. Liu, W.F. Shu, T. Nonfeer. Metal Soc., 27 (2017) 1656
26. M. Kang, M.E. Gross, A.A. Gewirth, J. Electrochem. Soc., 150 (2003) 292
27. Rene Winand, *J. Electrochem. Soc.*, 144 (1997) 428
28. M. Chomakova, S. Vitkova, *J. Appl. Electrochem*.,16 (1986) 669
29. John O. Dukovic, *J. Electrochem. Soc*., 137 (1990) 3748
30. C. Madore, *J. Electrochem. Soc.*, 143 (1996) 3927
31. W.R. Lin, S.H. Yang, Y.W. Sun, Y.M. Chen, J. He, C.B. Tang, Chin. J. Nonferrous Met., 27 (2017) 399
32. W. Szmaja, W. KozłOwski, K. Polański, J. Balcerski, M. Cichomski, J. Grobelny, M. Zieliński, E. Miękoś, *Mater. Chem. Phys*., 132 (2012) 1060